Searching for $H \to hh \to b\bar{b}\tau\tau$ in the 2HDM Type-I at the LHC

A. ARHRIB[1,2][*], S. MORETTI[3,4][†], S. SEMLALI[3,5][‡], C. H. SHEPHERD-THEMISTOCLEOUS[5][§], Y. WANG[6,7][¶], Q.S. YAN[8,9][‖]

[1] *Abdelmalek Essaadi University, Faculty of Sciences and Techniques, B.P. 2117 Tétouan, Tanger, Morocco.*

[2] *Department of Physics and Center for Theory and Computation, National Tsing Hua University, Hsinchu, Taiwan 300.*

[3]*School of Physics and Astronomy, University of Southampton, Southampton, SO17 1BJ, United Kingdom.*

[4]*Department of Physics and Astronomy, Uppsala University, Box 516, SE-751 20 Uppsala, Sweden.*

[5]*Particle Physics Department, Rutherford Appleton Laboratory, Chilton, Didcot, Oxon OX11 0QX, United Kingdom.*

[6]*College of Physics and Electronic Information, Inner Mongolia Normal University, Hohhot 010022, PR China.*

[7]*Inner Mongolia Key Laboratory for Physics and Chemistry of Functional Materials, Inner Mongolia Normal University, Hohhot, 010022, China.*

[8]*Center for Future High Energy Physics, Chinese Academy of Sciences, Beijing 100049, P.R. China.*

[9]*School of Physics Sciences, University of Chinese Academy of Sciences, Beijing 100039, P.R. China.*

Abstract

Unlike other realisations of the 2-Higgs Doublet Model (2HDM), the so-called Type-I allows for a very light Higgs boson spectrum. Specifically, herein, the heaviest of the two CP-even neutral Higgs states, H, can be the one discovered at the Large Hadron Collider (LHC) in 2012, with a mass of ≈ 125 GeV and couplings consistent with those predicted by the Standard Model (SM). In such a condition of the model, referred to as 'inverted mass hierarchy', the decay of the SM-like Higgs state into pairs of the lightest CP-even neutral Higgs boson, h, is possible, for masses of the latter ranging from $M_H/2 \approx 65$ GeV down to 15 GeV or so, all compatible with experimental constraints. In this paper, we investigate the scope of the LHC in accessing the process $gg \to H \to hh \to b\bar{b}\tau\tau$ by performing a Monte Carlo (MC) analysis aimed at extracting this signal from the SM backgrounds, in presence of a dedicated trigger choice and kinematic selection. We prove that some sensitivity to such a channel exists already at Run 3 of the LHC while the High-Luminosity LHC (HL-LHC) will be able to either confirm or disprove this theoretical scenario over sizable regions of its parameter space.

---

[*]a.arhrib@gmail.com

[†]s.moretti@soton.ac.uk; stefano.moretti@physics.uu.se

[‡]souad.semlali@soton.ac.uk

[§]claire.shepherd@stfc.ac.uk

[¶]wangyan@imnu.edu.cn

[‖]yanqishu@ucas.ac.cn

1 Introduction

In the SM of particle physics, it is well known that the Higgs boson [1, 2] is responsible for the generation of fermion and gauge boson masses through what is called Spontaneous Symmetry Breaking (SSB) [3, 4]. Such a mechanism also predicts a self-interaction for the Higgs state.

The measurement of such a self-coupling is the only experimental way to understand the SSB mechanism and to reconstruct the Higgs potential responsible for it. This is an important (and challenging) task also because it can shed some light on possible Beyond the SM (BSM) effects that may affect Higgs self-couplings in general.

The LHC has started a new campaign of measurements after the recent upgrade, the so-called Run 3. This will involve, among other things, measuring ever more precisely the coupling of the SM-like Higgs boson to other SM particles or even progressing towards the measurement of its self-coupling. The LHC is also capable of measuring new decays of the SM-like Higgs boson into non-SM particles. Current results from the ATLAS and CMS experiments indicate that the measured SM-like Higgs signal rates in all channels agree well with the SM theoretical predictions at the $\sim 2\sigma$ level [5, 6]. However, there are several pieces of evidences, both theoretical (the hierarchy problem, the absence of gauge coupling unification, etc.) and experimental (neutrino masses, the matter-antimatter asymmetry, etc.), which indicate that the SM could not be the ultimate description of Nature but should be viewed as a low-energy effective theory of some more fundamental one yet to be discovered.

There exist several BSM theories that address these weaknesses of the SM while identifying the 125 GeV scalar particle as a part of an extended scalar sector. One of the simplest extensions of the SM is the 2HDM, which contains two Higgs doublets, Φ_1 and Φ_2, which give masses to all fermions and gauge bosons. The particle spectrum of the 2HDM is as follows: two CP-even (h and H, with $m_h < m_H$, one of them being identified with the SM-like Higgs boson with mass 125 GeV: H in our case), one CP-odd (A) and a pair of charged ($H^\pm$) Higgs bosons.

According to the latest experimental results from both ATLAS and CMS, the presence of non-SM decay modes of the SM-like Higgs boson is not completely ruled out. Both experiments have set upper limits on the Branching Ratio (BR) of such non-SM decays which are 12% for ATLAS [5] and 16% for CMS [6]. The LHC experiments are expected to soon constrain the BRs of such non-SM decays beyond the 5-10% level using indirect measurements [7, 8]. There exist several BSM models that possess such non-SM decays of the SM-like Higgs boson: non-minimal scenarios of Supersymmetry [9] such as the Next-to-Minimal Supersymmetric Standard Model and new Monimal Supersymmetric Standard Model (NMSSM/mMSSM) [10–13], models for Dark Matter (DM) [14–17], scenarios with first order Electro-Weak (EW) phase transitions [18, 19] and an extended Higgs sector [20, 21]. It is then crucial to use LHC Higgs measurements to test BSM models that predict such exotic SM-like Higgs decays (i.e., into non-SM particles). In the 2HDM, if the heavy CP-even H is the observed SM-like Higgs boson, then H can decay into a pair of light CP-even Higgs states, $H \rightarrow hh$, or CP-odd ones, $H \rightarrow AA$. The phenomenology of such decays of the observed SM-like Higgs boson is studied in Refs. [22–25] for the case of the 2HDM, with an emphasis on the so-called Type-I (see below).

Following the discovery of the SM-like Higgs boson by ATLAS and CMS at the LHC in 2012, there have been several experimental searches for exotic decays of the SM-like Higgs through four fermions final states: $pp \rightarrow H \rightarrow XX \rightarrow f_1 f_1 f_2 f_2$, where $f_{1,2}$ are 2 light fermions such as muons, taus or bottom quarks. Such a search clearly benefits from the large cross-section

$\sigma(pp \to H)$ as well as from the large BR of the exotic SM-like Higgs decay $H \to hh$ that could reach up to 10% in some BSM scenarios. In that spirit, the ATLAS and CMS collaborations have performed several searches looking for $\tau\tau\tau\tau$ [26, 27], $\tau\tau\mu\mu$ [26, 28–30], $b\bar{b}\mu\mu$ [26, 31, 32], $b\bar{b}\tau\tau$ [33, 34], $eeee$ [35], $ee\mu\mu$ [35] and $\mu\mu\mu\mu$ [35–39], which have enabled one to set an upper limit on the BR of the X decay into any given 2 light fermions.

Motivated by the recent search for $b\bar{b}\tau\tau$ final states conducted by the CMS experiment [33, 34], herein, we would like to address the study of signal and background for such a final state within the so-called 2HDM Type-I. We first demonstrate that, within this framework, the production rate of $b\bar{b}\tau\tau$ via the process $\sigma(pp \to H) \times \mathrm{BR}(H \to hh) \times \mathrm{BR}(h \to b\bar{b}) \times \mathrm{BR}(h \to \tau\tau)$ could be substantial and then perform a feasibility study based on a signal-versus-background analysis using standard Monte Carlo (MC) simulation tools. It is found that the interesting parameter space could be either confirmed or disproved by a large data set (say 3000 fb^{-1}), which can be attained at the High Luminosity LHC (HL-LHC) [40], with possible hints of such a signal already at Run 3 of the LHC (for 300 fb^{-1}).

The paper is organised as follows: in section 2 we give a brief review of the 2HDM and describe the theoretical and experimental constraints that are used. In section 3, we present some general features of the SM-like Higgs boson decays into two light Higgs bosons and further into $b\bar{b}\tau\tau$ final states over the parameter space of the inverted mass hierarchy scenario of the 2HDM Type-I. In section 4, we perform a detailed MC study of the feasibility of the signal process $gg \to H \to hh \to b\bar{b}\tau\tau$ at the current Run 3 of the LHC and future HL-LHC stages. In section 5, we end this work with some conclusions.

2   Theoretical and Experimental Constraints

The 2HDM is obtained by extending the Higgs sector of the SM with an additional Higgs doublet field. Assuming that Φ_i $(i = 1, 2)$ are the two $SU(2)_L$ Higgs doublets and $v_{1,2}$ are their Vacuum Expectation Values (VEVs), the most general renormalisable potential which is invariant under $SU(2)_L \times U(1)_Y$ is given by [21]:

$$V_{\mathrm{Higgs}}(\Phi_1, \Phi_2) = \lambda_1(\Phi_1^\dagger\Phi_1)^2 + \lambda_2(\Phi_2^\dagger\Phi_2)^2 + \lambda_3(\Phi_1^\dagger\Phi_1)(\Phi_2^\dagger\Phi_2) + \lambda_4(\Phi_1^\dagger\Phi_2)(\Phi_2^\dagger\Phi_1) + \tag{1}$$

$$+\frac{1}{2}\left[\lambda_5(\Phi_1^\dagger\Phi_2)^2 + \mathrm{h.c.}\right] + m_{11}^2\Phi_1^\dagger\Phi_1 + m_{22}^2\Phi_2^\dagger\Phi_2 + \left[m_{12}^2\Phi_1^\dagger\Phi_2 - \mathrm{h.c.}\right].$$

By hermiticity, $\lambda_{1,2,3,4}$ as well as m_{11}^2 and m_{22}^2 are all real-valued. The parameters λ_5 and m_{12}^2 can be complex and can generate CP violation in the Higgs sector. However, in what follows, we assume that there is no such phenomenon.

After EW Symmetry Breaking (EWSB) takes place, from the 8 degrees of freedom initially present in Φ_1 and Φ_2, 3 are taken up by the ensuing Goldstone bosons to give masses to the gauge bosons $W^\pm$ and Z, so we are eventually left with 5 physical Higgs states. A pair of charged Higgs $H^\pm$, a CP-odd A and two CP-even states H and h (with $m_h < m_H$), as mentioned. One of the neutral CP-even Higgs states has to be identified with the 125 GeV SM-like Higgs particle observed at the LHC. In the present study, as intimated, we will assume $m_H = 125$ GeV while $m_h < m_H/2$.

The whole Higgs sector of the 2HDM is then parameterised by 7 parameters: e.g.,

$$m_{H^\pm}, \ m_A, \ m_H, \ m_h, \ \alpha, \ \beta \text{ and } m_{12}^2, \tag{2}$$

where α is the mixing angle between the CP-even components of the neutral Higgs states of the doublet fields while β is the mixing between the CP-odd components and is given by $\tan\beta = v_2/v_1$. As we are considering the scenario where H state is the 125 GeV scalar, the SM (alignment) limit is recovered when $\cos(\beta - \alpha) \approx 1$.

From the above Higgs potential, one can derive, in particular, the triple Higgs coupling Hhh needed for our analysis, as follows [41, 42]:

$$Hhh = -\frac{g c_{\beta-\alpha}}{2 m_W s_{2\beta}^2} \left[(2m_h^2 + m_H^2) s_{2\alpha} s_{2\beta} - 2(3s_{2\alpha} - s_{2\beta}) m_{12}^2 \right], \tag{3}$$

where s_x and c_x are shorthand notations for $\sin x$ and $\cos x$, respectively. The coupling Hhh is proportional to $\cos(\beta - \alpha)$ which is close to unity in our scenario with H being the observed SM-like Higgs boson, as explained.

In the Yukawa sector, if we proceed to EWSB like in the SM, we end up with Flavour Changing Neutral Currents (FCNCs) at tree level. Such dangerous FCNCs can, however, be avoided by imposing a discrete Z_2 symmetry [43] by coupling each fermion type to only one of the Higgs doublets. As a consequence, there are four types of 2HDM [21], of which, in this study, we are interested only in the so-called Type-I, wherein only the doublet Φ_2 couples to all fermions exactly as in the SM [21].

The neutral Higgs couplings to fermions can be obtained from the Yukawa Lagrangian and are given by [21]:

$$-\mathcal{L}_{\text{Yukawa}} = \sum_{f=u,d,l} \frac{m_f}{v} \left(\frac{\cos\alpha}{\sin\beta} \bar{f} f h + \frac{\sin\alpha}{\sin\beta} \bar{f} f H \right). \tag{4}$$

As one can read from the above Lagrangian term, the CP-even neutral Higgs couplings to quarks and leptons are similar in the 2HDM Type-I, since both are proportional to $\frac{1}{\sin\beta} \propto \frac{1}{\tan\beta}$: in particular, the H couplings to all fermions are suppressed if $\tan\beta \gg 1$.

The parameter space of the 2HDM (whatever the Type) is limited by both theoretical and experimental constraints. The theoretical ones that have been imposed on the Higgs potential are as follows.

- Perturbativity constraints imply that all quartic coefficients of the Higgs potential satisfy the condition $|\lambda_i| \leq 8\pi$ $(i = 1, ...5)$ [21].

- Perturbative unitarity constraints require that $2 \to 2$ scattering processes involving Higgs and gauge bosons remain unitary at high energy [44–46].

- Vacuum stability conditions require the Higgs potential to be bounded from below when the Higgs fields become large in any direction of the field space [47].

We have used the public code 2HDMC-1.7.0 [48] to check the above theoretical constraints.

We also take into account experimental constraints from Higgs analyses at lepton and hadron colliders (LEP, Tevatron and LHC) as well as EW Precision Observables (EWPOs). Limits from flavour physics observables are also considered. Specifically, we have proceeded as follows.

- Exclusion limits at 95% Confidence Level (CL) from Higgs analyses at the aforementioned colliders are implemented via HiggsBounds-5.9.0 [49] and HiggsSignals-2.6.0 [50].

- We impose compatibility with the EWPOs by requiring the computed S, T and U values [51–53] be within 2σ of the SM fit of [54], taking into account the full correlations among the three parameters.

- Constraints from B-physics observables are taken into account by using the public code SuperIso v4.1 [55], in particular, we have used the following measurements:

  - $\mathrm{BR}(\overline{B} \to X_s\gamma)|_{E_\gamma < 1.6 \text{ GeV}} = (3.32 \pm 0.15) \times 10^{-4}$ [56],
  - $\mathrm{BR}(B_s \to \mu^+\mu^-)_{\text{(LHCb)}} = (3.09^{+0.46}_{-0.43}) \times 10^{-9}$ [57,58],
  - $\mathrm{BR}(B_s \to \mu^+\mu^-)_{\text{(CMS)}} = (3.83^{+0.38}_{-0.36}) \times 10^{-9}$ [59],
  - $\mathrm{BR}(B^0 \to \mu^+\mu^-)_{\text{(LHCb)}} = (1.2^{+0.8}_{-0.7}) \times 10^{-10}$ [57,58],
  - $\mathrm{BR}(B^0 \to \mu^+\mu^-)_{\text{(CMS)}} = (0.37^{+0.75}_{-0.67}) \times 10^{-10}$ [59].

3 Numerical Results

As mentioned repeatedly, in this study, we focus on the inverted mass hierarchy scenario, where the heaviest Higgs is identified as the observed 125 GeV at the LHC. We then scan randomly the 2HDM parameters over the ranges of Tab. 1.

Parameter	m_h (GeV)	m_A (GeV)	$m_{H^\pm}$ (GeV)	$\sin(\beta - \alpha)$	$\tan\beta$	m_{12}^2 (GeV^2)
Range	[10, 62]	[62 , 100]	[96, 200]	[-0.25, -0.05]	[2, 25]	$m_h^2 \cos\beta \sin\beta$

Table 1: The input parameters of the 2HDM are tabulated and their scan ranges given. (Note that we have fixed $m_H = 125$ GeV.)

Upon meeting the theoretical requirements and the constraints derived from past and ongoing experimental studies, described in section 2, we illustrate in Figs. 1 and 2 the BRs for different decay modes of the light Higgs: $h \to \gamma\gamma$, $b\bar{b}$ and $\tau\tau$. Away from the fermiophobic limit, where the light Higgs couplings to fermions (κ_f^h) are very suppressed $(c_\alpha/s_\beta \to 0)$ and the di-photon decay of the light Higgs state can become significant, the total width of the h state is clearly dominated by $h \to b\bar{b}$, over the entire 2HDM Type-I parameter space, with a BR of 85%, followed by the decay into $\tau\tau$ with BR of order $\sim 8\%$. The decay rate of $h \to b\bar{b}$ drops to 45% when κ_f^h approaches very small values $(\lesssim 0.001)$ and m_h is around 15 GeV. Furthermore, the partial width $\Gamma(h \to b\bar{b})$ exhibits a suppression near the $2m_b$ threshold and, therefore, $h \to \gamma\gamma$ can closely compete with $h \to b\bar{b}$ there.

Fig. 3 shows the overall cross-section of the process $pp \to H \to hh \to b\bar{b}\tau\tau$, wherein the main channel for producing the SM-like Higgs boson H is the gluon-gluon fusion mechanism. Here, $\mathrm{BR}(h \to b\bar{b})$, $\mathrm{BR}(h \to \tau\tau)$ and $\mathrm{BR}(H \to hh)$ are also displayed. Since the decay width of the SM-like Higgs (Γ_H) is of the order of a few MeV $(\Gamma_H^{\text{ATLAS}} = 4.6^{+2.6}_{-2.5}$ MeV [60] and $\Gamma_H^{\text{CMS}} = 3.2^{+2.4}_{-1.7}$ MeV [61]), one can assume the Narrow Width Approximation (NWA)[1] and then write the complete production times decay cross-section as follows:

$$\sigma_{b\bar{b}\tau\tau} = \sigma(gg \to H) \times \mathrm{BR}(H \to hh) \times \mathrm{BR}(h \to b\bar{b}) \times \mathrm{BR}(h \to \tau\tau), \tag{5}$$

---

[1]The same applies to the h state, which would be even narrower.
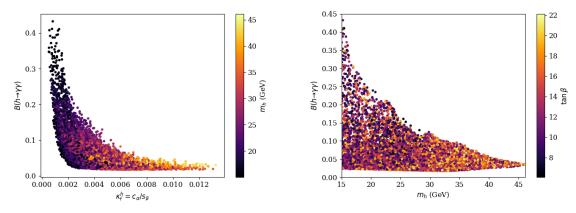
Figure 1: BR($h \to \gamma\gamma$) as a function of κ_f^h vs. m_h (left panel) and as a function of m_h vs. $\tan\beta$ (right panel) vs. m_h.
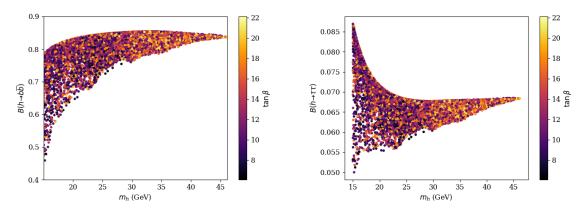

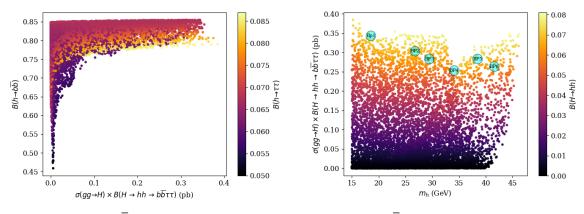Figure 2: BR($h \to b\bar{b}$) (left panel) and BR($h \to \tau\tau$) (right panel) vs. m_h and $\tan\beta$.

Figure 3: BR($h \to b\bar{b}$) as a function of $\sigma(gg \to H \to hh \to b\bar{b}\tau\tau)$ vs. BR($h \to \tau\tau$) (left panel) and $\sigma(gg \to H \to hh \to b\bar{b}\tau\tau)$ as a function of m_h vs. BR($H \to hh$) (right panel).

where $\sigma(gg \to H)$ is the H production rate computed (here) at Leading Order (LO) using SusHi 1.7.0 [62–64] at the center-of-mass energy of 13 TeV. (The N³LO QCD corrections will be considered through a K-factor [65, 66], see below.) As shown previously in Eq. (3), the trilinear Higgs coupling Hhh is proportional to $\cos(\beta - \alpha)$. In the inverse mass hierarchy configuration of the 2HDM Type-I, current data drive $\cos(\beta-\alpha)$ to closely approach 1[2] and thus

---

[2]The allowed values of the SM-like Higgs couplings to vector bosons, $\kappa_V^H = \cos(\beta - \alpha)$, $V = W^\pm, Z$, lie very close to 1, with a deviation of 2% from the SM values.

BR($H \to hh$) is not suppressed. However, it is observed that the BR of the SM-like Higgs boson (H) decaying into a pair of light Higgs bosons (hh) remains below 10% when the decay channel becomes kinematically accessible. This limitation arises from the precise measurements of the Higgs boson couplings, which impose stringent constraints on exotic decays of the Higgs boson, i.e., into BSM particles and/or undetected final states (invisible, for short). As mentioned, the ATLAS and CMS collaborations have set, respectively, an upper limit of 12% [5] and 16% [6] on BR($H \to$ invisible) at 95% CL, using LHC Run 2 data. Recently, the ATLAS collaboration also performed a combination of Run 1 and 2 direct searches for invisible Higgs decays, where several production modes of the SM-like Higgs boson are considered [67]. An upper bound of 10.7% (7.7%) on BR($H \to$ invisible) at the 95% CL has been observed (expected). The CMS collaboration has also lately presented the combination of a search for $H \to$ invisible with the SM-like Higgs state produced in association with a top-antitop pair (i.e., $pp \to t\bar{t}H$) or a vector boson (i.e., $pp \to VH$) using 138 fb^{-1} of data from both Run 1 and 2: the combined upper limit on BR($H \to$ invisible) is 15% at 95 CL [68]. Compatibly with these constraints, we find that the cross-section for the process $gg \to H \to hh \to b\bar{b}\tau\tau$ reaches its maximum value of 0.4 pb when BR($h \to b\bar{b}$), BR($h \to \tau\tau$) and BR($H \to hh$) are at their maximum values. Over the parameter region allowing for this, we have marked several Benchmark Points (BPs) amenable to MC simulation, which are listed in Tab. 2.

An additional scan is then performed with fixed values of $m_{H^{\pm}}$ = 165.58 GeV, m_A = 98.9 GeV, $\sin(\beta - \alpha)$ = −0.10, m_{12}^2 = 154 GeV^2 while m_h and $\tan\beta$ are varied randomly as shown in Tab. 1. We show in the left panel of Fig. 4 the allowed region resulting from passing
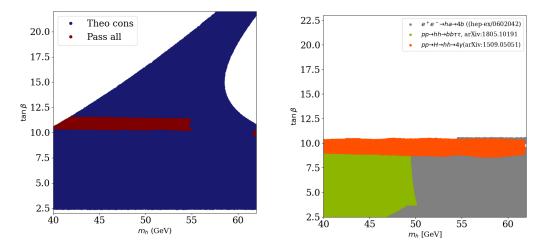

Figure 4: Allowed (left panel) and excluded (right panel) parameter space over the (m_h, $\tan\beta$) plane. Here, $m_{H^{\pm}}$ = 165.58 GeV, m_A = 98.9 GeV, $\sin(\beta - \alpha)$ = −0.10, m_{12}^2 = 154 GeV^2.

the theoretical constraints, indicated by blue colour. The points that meet the theoretical requirements and also align with experimental data are highlighted in red colour. To gain a better understanding of this restricted parameter space, which is limited to a narrow range of values of $\tan\beta$, specifically between 9 and 11.50, we illustrate in the right panel of Fig. 4 the excluded regions and the corresponding searches. For values of $\tan\beta$ below 9, the CMS search for exotic decays in the $b\bar{b}\tau\tau$ [34] final state has excluded the mass range where $m_h < 50$ GeV whereas the region where $m_h > 50$ GeV is excluded by the LEP search for $e^+e^- \to hA \to b\bar{b}b\bar{b}$ [69]. Additionally, an ATLAS search for events with at least three photons (i.e., 3γ) targeting the process $pp \to H \to hh \to 4\gamma$ [70] has led to the exclusion of the parameter space with $\tan\beta > 9$ and 40 GeV < m_h < 62.5 GeV.

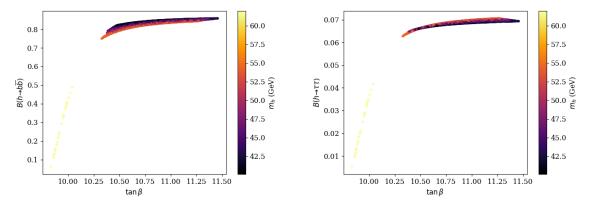Figure 5: BR($h \to b\bar{b}$) (left panel) and BR($h \to \tau\tau$) (right panel) as a function of $\tan\beta$ vs. m_h. Here, $m_{H^\pm} = 165.58$ GeV, $m_A = 98.9$ GeV, $\sin(\beta - \alpha) = -0.10$, $m_{12}^2 = 154$ GeV^2.

We show in Fig. 5 the different BRs within the described parameter space. Similarly to Fig. 1, the dominant channel within the parameter space where $m_h < 60$ GeV is $h \to b\bar{b}$, with a BR that can reach up to 85%. The second prominent channel is $h \to \tau\tau$ with a BR that goes up to 8%. Another interesting observation is that the fermionic decay rates of $h \to b\bar{b}$ and $\tau\tau$ remain relatively unaffected by $\tan\beta$ variations. For large $\tan\beta$, the Yukawa couplings[3] become suppressed, leading the BRs of the light Higgs state decaying into fermions to become fairly independent on the values of $\tan\beta$ within the considered parameter space.
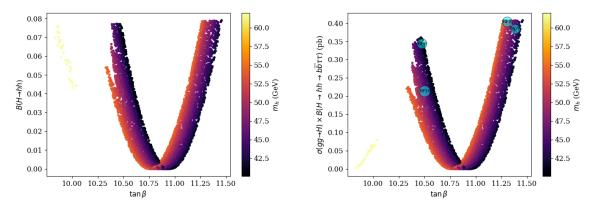

Figure 6: BR($h \to hh$) (left panel) and $\sigma(gg \to H) \times$ BR($H \to hh \to b\bar{b}\tau\tau$) (right panel) as a function of $\tan\beta$ vs. m_h.

In Fig. 6, we present the production cross-section of the SM-like Higgs state H times its decay BR into $b\bar{b}\tau\tau$ via hh, i.e., $\sigma(gg \to H) \times$ BR($H \to hh \to b\bar{b}\tau\tau$), within the specified parameter space. The maximum value of this product is observed to be 0.4 pb, which occurs, again, when BR($H \to hh$), BR($h \to \tau\tau$) and BR($h \to b\bar{b}$) all reach their maximum values within the considered parameter space. Similarly to the previous scenario, we have selected a few BPs to perform a MC simulation. These BPs are carefully chosen to cover a range of interesting scenarios and to explore various aspects of the model, see Tab. 2.

---

[3]Notice that $\kappa_h^f = \sin(\beta - \alpha) + \cot\beta \cos(\beta - \alpha) \approx \sin(\beta - \alpha)$ for large $\tan\beta$, with $\sin(\beta - \alpha) = -0.10$.

4 Feasibility Study at the LHC Run 3

In our MC analysis, we focus on the $b\bar{b}\tau\tau$ final state, where both τ leptons decay into either an electron or a muon, along with their respective neutrinos. To distinguish between the decays of the τ particles, we use the short-hand notations τ_e and τ_μ to represent the channels $\tau \to e\bar{\nu}_e\nu_\tau$ and $\tau \to \mu\bar{\nu}_\mu\nu_\tau$, respectively. The final states $\tau_e\tau_e$ and $\tau_\mu\tau_\mu$ are neglected in order to suppress the significant contamination from Drell-Yan (DY) background events. In Fig. 7, we present the Feynman diagram of the signal process, where effective vertices are considered for the gluon-gluon-Higgs coupling and for leptonic tau decay [71].
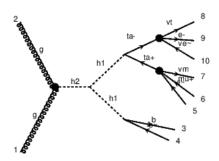
Figure 7: Feynman diagram for the process $gg \to H \to hh \to b\bar{b}\tau_e\tau_\mu$. Here, $h_2 \equiv H$ and $h_1 \equiv h$.

We use `MadGraph-v.3.4.2` [72] to generate parton-level events of both signal and background processes. To account for the τ decays, we use the `TauDecay` library [71][4]. The QCD corrections are taken into account by using K-factors for (what we will prove to be) the two main background processes $Z(\to \tau_e\tau_\mu)b\bar{b}$ [73] and $t\bar{t}$ [74]: specifically, $K = 1.4$ for both $b\bar{b}Z$ and $t\bar{t}$. The K-factor for the signal production process $gg \to H$ is taken as $K = 2.5$, which includes the N^{3}LO QCD corrections of Refs. [65, 66]. We then pass the events to `PYTHIA8` [75] for parton showering, fragmentation/hadronisation and heavy flavour decays. Then, we use `Delphes-3.5.0` [76] with a standard CMS card to simulate the detector response. Finally, we employ `MadAnalysis 5` [77] to apply cuts and to conduct the kinematic analysis. As mentioned already, the BPs and the corresponding parameter values used to generate MC samples of events for the signal process are given in Tab. 2, where, as usual, the collision energy at the proton-proton level is assumed to be 13 TeV.

In order to generate signal and background events efficiently, we apply the following kinematic cuts at parton level:

$p_T(b) > 10\,\text{GeV}$, $p_T(l) > 5\,\text{GeV}$, $E_T^{\text{miss}} > 5\,\text{GeV}$, $|\eta(b,l)| < 2.5$, $\Delta R(ll, bl, bb) > 0.3$, H_T[5] $< 70\,\text{GeV}$.

The LO cross-sections of all background processes considered in our initial MC analysis are given in Tab. 3. As intimated, it is found that the dominant background processes arise from top pair production ($t\bar{t}$) and $Z(\to \tau_e\tau_\mu)b\bar{b}$, so that we will simulate only these two processes in our final (detector level) analysis.

---

[4]The `TauDecay` package has been added to the UFO file of the 2HDM Type-I.

[5]Where H_T is computed over all partons.

BP	m_h (GeV)	m_a (GeV)	$m_H^\pm$ (GeV)	$\sin(\beta-\alpha)$	$\tan\beta$	$\sigma_{b\bar{b}\tau\tau}$ (pb)	BR($H \to hh$)	BR($h \to b\bar{b}$)	BR($h \to \tau\tau$)
BP1	17.67	73.70	184.51	-0.053	19.68	0.34	0.07	0.81	0.076
BP2	25.9	80.61	171.88	-0.064	16.71	0.3	0.068	0.84	0.068
BP3	28.56	94.46	155.45	-0.11	9.09	0.28	0.065	0.85	0.067
BP4	33.20	88.29	99.75	-0.076	14.42	0.25	0.058	0.85	0.067
BP5	37.56	88.88	188.64	-0.064	16.45	0.28	0.072	0.8	0.064
BP6	40.68	88.37	144.39	-0.054	19.37	0.26	0.063	0.82	0.066
BP7	47.27	98.91	165.58	-0.10	11.34	0.38	0.074	0.85	0.074
BP8	54.03	98.91	165.58	-0.10	11.28	0.40	0.083	0.84	0.07
BP9	43.44	98.91	165.58	-0.10	10.43	0.34	0.077	0.80	0.065
BP10	49.39	98.91	165.58	-0.10	10.41	0.21	0.056	0.78	0.065

Table 2: The cross-sections $\sigma_{b\bar{b}\tau\tau} \equiv \sigma(gg \to H) \times \mathrm{BR}(H \to hh) \times \mathrm{BR}(h \to b\bar{b}) \times \mathrm{BR}(h \to \tau\tau)$ for our BPs are given for the collision energy $\sqrt{s}$ = 13 TeV alongside the BRs for the decay channels $H \to hh$, $h \to b\bar{b}$ and $\tau\tau$. The unit of all masses is GeV. Here, m_H = 125 GeV, and in the values of cross-section $\sigma_{b\bar{b}\tau\tau}$ the K-factor has been taken into consideration.

Background process	σ (pb)
$pp \to Z(\to b\bar{b})Z(\to ll)$, $l = (e,\ \mu,\ \tau_{e,\ \mu})$	0.009 pb
$pp \to Z(\to ll)b\bar{b}$, $l = (e,\ \mu,\ \tau_{e,\ \mu})$	6.1 pb
$pp \to Z(\to b\bar{b})ll$, $l = (e,\ \mu,\ \tau_{e,\ \mu})$	0.015 pb
$pp \to ZW^\pm j$, $W^\pm \to l\nu_l$ $(l = e,\ \mu, \tau_{e,\ \mu})$	0.0051 pb
$pp \to t\bar{t} \to e^\pm\mu^\mp b\bar{b} + E_T^{\mathrm{miss}}$	0.28 pb

Table 3: The LO background cross-sections are given for the collision $\sqrt{s}$ = 13 TeV. The K-factors mentioned in the text has not been included here but will be used to compute the final significances, albeit limitedly to the second and last processes (i.e., the two dominant noises).

4.1 Parton Level Analysis

In Fig. 8, the p_T distributions of the leading and subleading leptons as well as of the b-(anti)quarks for the signal are displayed. These spectra provide insights into the transverse momentum of final-state particles involved in the signal process, in order to guide our final analysis at detector level.

On the one hand, it is observed that the leading and subleading leptons originating from the light Higgs decay (recall that m_h < 62.5 GeV) tend to have lower transverse momentum, indicating that they are relatively softer when compared with the leading (subleading) b-(anti)quarks from the same light Higgs state (owing to neutrinos carrying away energy). In particular, the peak value of p_T of the subleading lepton is less than 10 GeV, which means a stiff (detector level) cut on $p_T(l)$ may lead to a severe loss of signal events. On the other hand, since the b-tagging efficiency decreases with p_T, then one should expect that a stiff (detector level) cut on, especially, the subleading b-jet can also lead to a severe loss of signal events. In short, these factors call for a dedicated trigger choice, that we will illustrate below.

In Fig. 9, we show the leading (subleading) lepton and b-(anti)quark of different background processes at parton level. It is observed that the subleading lepton from $Z(\to b\bar{b})\tau_e\tau_\mu$ can be very soft, just like the subleading lepton from the signal events. Similarly, the subleading b-(anti)quark from $Z(\to \tau_e\tau_\mu)b\bar{b}$ can be very soft, which can then mimic the subleading b-(anti)quark of the signal events. Thus, this renders even more important the accurate choice of a dedicated trigger for this analysis. However, as intimated, from Tab. 3, it is clear that the dominant background processes are $pp \to Z(\to \tau_e\tau_\mu)b\bar{b}$ and $pp \to t\bar{t}$. Therefore, in order
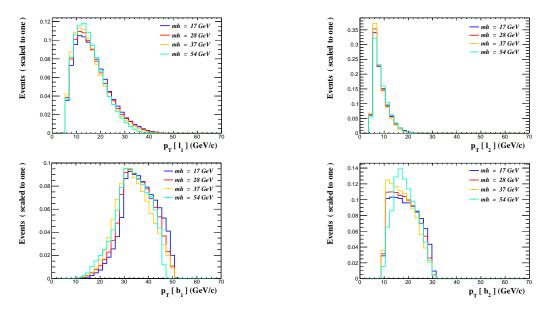
Figure 8: The p_T distributions of the leading (subleading) lepton (top panel) and leading (subleading) b-(anti)quark (bottom panel) for different signal BPs at are shown at parton level, see Tab. 3.
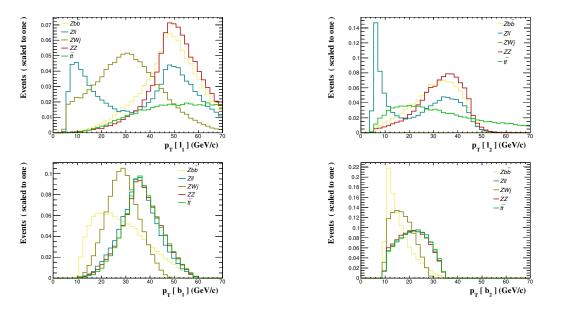

Figure 9: The p_T distributions of the leading (subleading) lepton and b-(anti)quark of different background processes are shown at parton level, see Tab. 3.

to discover the signal process, the key task is to ultimately suppress these two backgrounds. Armed with the knowledge acquired at the parton level, we will investigate below how to suppress these two types of noise most effectively at the detector level.

4.2 Detector Level Analysis

We only consider events with two b-jets and two leptons of different flavour with opposite charges (i.e., $e^{\mp}\mu^{\pm}$) in the final state. Given that both (leading and subleading) leptons in the signal events are soft, as illustrated in Fig. 10, it will be necessary to suitably adjust the transverse momentum (p_T) thresholds of the leading electron (e) and subleading muon (μ).

By reducing these p_T thresholds, one can include more signal events and then increase the acceptance so to mitigate the potential significant loss of signal events due to the softness of the leptons, especially the subleading one. Consequently, the trigger choice could lead to a more comprehensive view of the final state and potentially improve the overall sensitivity of the analysis.
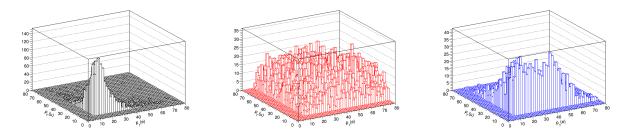

Figure 10: Correlations between the p_T of the leading and subleading leptons for signal (black), $t\bar{t}$ (red) and $b\bar{b}Z(\rightarrow \tau_e\tau_\mu)$ (blue) are shown at detector level.

Events featuring tau decays into leptons ($\tau_e\tau_\mu$) are collected by electron and muon triggers. The CMS cross trigger [78, 79] relies on the presence of both an electron (e) and a muon (μ), where the leading lepton has a p_T threshold of 23 GeV and the subleading one has a $p_T > 12$ GeV for an electron or 8 GeV for a muon [32, 34]. This trigger is limited by p_T thresholds in the Level-1 (L1) trigger selection due to the limited L1 bandwidth available. The double electron trigger is similarly limited. Recently, in Run 3, CMS has overcome this limitation for electron pairs that are close together, for example from B meson decays, by placing tighter topological selection on the two electrons L1 objects. This borrows from established approaches already used in double muon triggers searching for low p_T muons from B meson decays. By applying similar topological approaches to an electron muon trigger, it would seem possible to develop a reasonably efficient L1 selection targeting 10 GeV close by electron muon pairs with a rate in the ~ 2 – 5 kHz range at nominal Run 3 luminosities. A L1 selection with such a bandwidth is feasible to be deployed in Run 3 if there is sufficient will on the experiment's side to do so and would be easily achievable at the HL-LHC. At the high level trigger (HLT) selection stage, the rate should be manageable and if not, scouting and parking techniques [80, 81] can be used if the rate of the selection is too much to be included in the standard physics stream. Electrons and muons from τ decays are then selected after satisfying the following requirements:

$$p_T^e > 10 \text{ GeV}, \ p_T^\mu > 8 \text{ GeV}, \ |\eta^e| < 2.4, \ |\eta^\mu| < 2.4.$$

Lepton candidates must also satisfy isolation criteria, which ensure that the amount of activity in a cone of radius $R = 0.4$ centered on the muon (electron) direction is smaller than 20% (15%) of p_T^μ (p_T^e). For the jets candidates, we employ the anti-k_T algorithm [82] to cluster detector-level objects with a jet radius parameter $\Delta R = 0.4$ and $p_{T,j}^{\min} = 10$ GeV (for both light- and b-jets)[6]. All events are required to have two b-tagged jets with $p_T(b_1/b_2) > 10$ GeV (where $p_T(b_{1 \ (2)})$ represents the b-jet with highest (lowest) p_T) and $|\eta^b| < 2.4$[7]. The reconstruction of b-jet with jets of $p_T < 20$ GeV might be very challenging due to the degradation in b-tagging efficiency over lower transverse momentum ranges, however, it is still worthwhile to investigate how the b-tagging efficiency changes in response to different p_T thresholds, so that we will do so below.

---

[6]Note that our results are rather stable against a different choice of jet clustering algorithm, like the Cambridge-Aachen one [83, 84].

[7]Jets are b-tagged with an average efficiency ($\varepsilon_{b/b}$) of ~ 60% (i.e., $\varepsilon_{b/b} = 0.85 \times \tanh(0.0025 \times p_T) \times (25.0/(1 + 0.063 \times p_T))$ [85], with p_T is the transverse momentum of the jet.)

To increase the sensitivity of our analysis, we will explore various kinematic distributions which include the invariant mass of the b-jets ($m_{b\bar{b}}$) as well as the constructed mass from the τ leptons decay products and the b-jets (m_T^H). These variables are typically low for signal events because the objects originate from a 125 GeV Higgs state. Conversely, they generally have higher values for background events, where the objects do not arise from a decay of a (rather light) resonance. Such kinematic features can serve to efficiently discern between signal and background events in our analysis.

Fig. 11 displays the invariant mass distribution of the b-jets for different BPs. Notably, $m_{b\bar{b}}$ aligns closely to the light Higgs mass (m_h) for each BP. We present in Fig. 12 the transverse
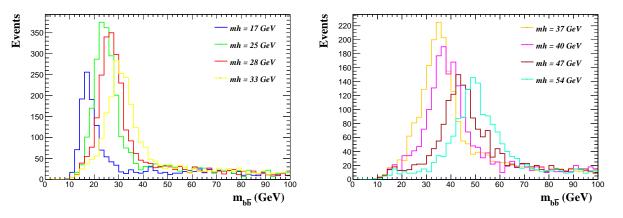

Figure 11: The distributions of $m_{b\bar{b}}$ for different BPs are shown at detector level.

mass distributions constructed from the two charged leptons and E_T^{miss}. As anticipated, the peak structure in these distributions is shifted from the expected light Higgs mass for the selected BPs ($m_T^{ll} \lesssim m_h$) due to the missing contribution of the neutrinos. The m_T^{ll} variable is defined from p_{ll} (the total four-momentum of the leptons) and E_T^{miss} as

$$m_T^{ll} = \sqrt{p_{ll}^0 E^0 - |p_{ll}^T||E^T|\cos(\phi_{ll,E_T^{\text{miss}}})}. \tag{6}$$

For the sake of convenience, we denote E_T^{miss} as (E^0, E^T, p_z), where p_z is the unknown z-component of the missing momentum and E^T is a 2D vector defined in the (x, y) plane perpendicular to the beam direction. Here, $\phi_{ll,E_T^{\text{miss}}}$ denotes the perpendicular angle between the di-lepton system and E_T^{miss}.
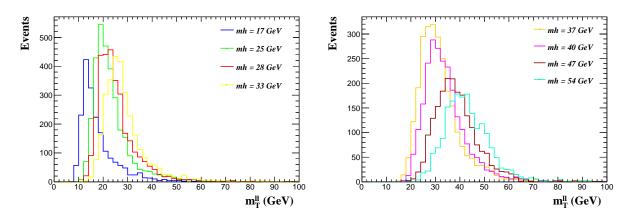

Figure 12: The distributions of m_T^{ll} for different BPs are shown at detector level.

In Fig. 13, we show the transverse mass constructed from the two b-jets, the two leptons and E_T^{miss}. The variable m_T^H is defined from the two b-jet four-momenta $p_{b\bar{b}} = p(b) + p(\bar{b})$, p_{ll}

12

and E_T^{miss}. To define m_T^H, we first express the visible momentum, which equals $p_{\mathrm{vis}} = p_{b\bar{b}} + p_{ll}$, so that we have

$$m_T^H = \sqrt{p_{vis}^0 E^0 - |p_{vis}^T||E^T|\cos(\phi_{\mathrm{vis},E_T^{\mathrm{miss}}})}\,, \qquad (7)$$

where $\phi_{\mathrm{vis},E_T^{\mathrm{miss}}}$ denotes the perpendicular angle between visible momentum and E_T^{miss}. Clearly, fully reconstructing the signal can yield a significant improvement in the signal-to-background ratio. Selecting events with low m_T^H will efficiently mitigate the background contamination arising from the $t\bar{t}$ process, which is characterised by a large missing transverse momentum.
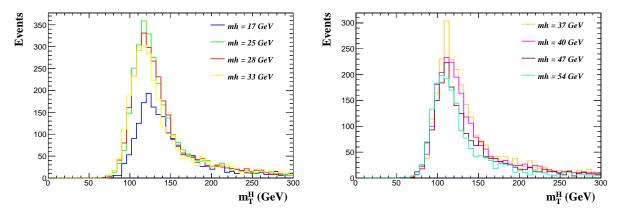

Figure 13: The distributions of m_T^H for different BPs are shown at detector level.

The requirement for precisely two b-tagged jets in each event is notably a tight condition due to the soft transverse momentum (p_T) spectrum of b-jets and the limited efficiency of the b-tagging algorithm. These b-tagging techniques [86, 87] operate at peak efficiency when b-jets possess a large transverse momentum of at least 20 GeV. However, at this threshold, a significant loss of the signal would occur particularly in scenarios involving low Higgs masses below 60 GeV as a result of the kinematics. Therefore, to examine how the efficiencies can change, especially the b-tagging one, we will compare the impact of the following three cuts, which we regard as pre-selection rules:

$$p_T(b_1/b_2) > 15/10 \text{ GeV}, \quad p_T(b_1/b_2) > 20/15 \text{ GeV}, \quad p_T(b_1/b_2) > 20/20 \text{ GeV}. \qquad (8)$$

The results are provided in Tabs. 4, 5 and 6, respectively. (In these tables, to estimate the number of events, we assume that the LHC collision energy at proton-proton level is $\sqrt{s} = 13$ TeV and the integrated luminosity is that of Run 3, i.e., 300 fb^{-1}.) Meanwhile, the leptons from τ decays are collected with thresholds at $p_T(e/\mu) = 10/8$ GeV, which can guarantee a sufficiently large fraction of signal events to be retained. We now discuss the effect of three pre-selections introduced in Eq. (8) in turn, each of which is supplemented by the same cutflow, which has been devised following the kinematic analysis performed at detector level.

In Tab. 4, we adopt the following pre-selection cuts:

$$p_T(b_1) > 15 \text{ GeV}, \ p_T(b_2) > 10 \text{ GeV}, \ p_T(e/\mu) = 10/8 \text{ GeV}. \qquad (9)$$

As stated above, several requirements on events are enforced. The first one is that each event contains exactly two leptons ($\ell^{\pm}\ell^{\mp} = e^{\pm}\mu^{\mp}$). Events with lepton-pair invariant mass with 10 GeV of the Z-boson mass are rejected ("m_Z-veto"). This cut will not affect the signal but can act on background events. Following the selection of 2 tagged b-jets, we apply an additional

selection criterion on the transverse mass (m_T^H) requiring that 65 GeV $< m_T^H <$ 125 GeV. This is reasonable as the Jacobian peak of the transverse mass of the SM-like Higgs boson is bound to be smaller than SM-like Higgs boson mass itself, m_H = 125 GeV. For the signal events, where both $b\bar{b}$ and $\tau\tau$ originate from the decay of the light Higgs, h, in principle, we expect the reconstructed masses $m_{b\bar{b}}$ and m_{ll}^T to be closely correlated. In reality, a major difference between the two reconstructed masses, as shown in Fig. 11 and Fig. 12, arises due to the z-component of the missing energy which is absent in m_{ll}^T, which prevents us from finding the precise invariant mass of the light Higgs boson decaying into $\tau\tau$. In order to quantify the difference between $m_{b\bar{b}}$ and m_{ll}^T, we have then introduced a new variable (Δm_h) i.e., $\Delta m_h \equiv (m_{b\bar{b}} - m_{ll}^T)/m_{ll}^T$. A cut on $\Delta m_h <$ 0.5 would help removing background events since in the latter there is no correlation between $m_{b\bar{b}}$ and $m_{\tau\tau}$. Lastly, we set cuts on m_T^{ll} and m_{bb} to be half of m_H in order to capture the SM-like Higgs boson decaying into two light Higgs bosons, $H \to hh$, in the signal events. Combining all kinematic information so far, we summarize in Tab. 4 the event rates after meeting the event selection requirements,

BP	BP1	BP2	BP3	BP4	BP5	BP6	BP7	BP8	BP9	BP10
m_h (GeV)	17.67	25.9	28.56	33.20	37.56	40.68	47.27	54.03	43.44	49.39
NoE($\mathcal{L}, \sigma$)	912.86	727.65	687.432	573.3	771.74	769.18	1086.62	1528.8	900.000	771.750
$e^\pm \mu^\mp$	156.934	151.874	141.094	114.84	146.44	136.2	160.54	204.94	151.226	111.163
m_Z-veto	156.934	151.874	141.094	114.84	146.44	136.2	160.54	204.94	151.226	111.163
2 b-jets	33.0	42.88	39.98	32.32	38.84	34.94	40.9	53.2	38.09	26.28
65 GeV $< m_T^H <$ 125 GeV	11.78	20.56	19.1	16.42	20.4	18.78	23.02	33.92	20.95	15.15
$\Delta m_h <$ 0.5	8.1	15.88	15.16	12.96	16.24	14.84	18.18	27.34	16.95	12.015
$m_T^{ll} <$ 62.5 GeV	8.1	15.86	15.14	12.94	16.24	14.84	18.18	27.18	16.63	11.98
$m_{bb} <$ 62.5 GeV	8.1	15.86	15.12	12.94	16.24	14.76	18.18	27.04	16.60	11.97

Table 4: Event rates of the signal with $\sqrt{s}$ = 13 TeV and integrated luminosity 300 fb^{-1} for different BPs are shown as a function of our cutflow. The pre-selection cuts are as given in Eq. (9).

Tab. 5 presents the results based on the following pre-selection cuts, while considering the same kinematic cuts as in Tab. 4:

$$p_T(b_1) > 20 \text{ GeV}, \ p_T(b_2) > 15 \text{ GeV}, \ p_T(e/\mu) = 10/8 \text{ GeV}. \tag{10}$$

Here, the same comments on the event kinematics of the signal apply as for the previous table.

BP	BP1	BP2	BP3	BP4	BP5	BP6	BP7	BP8	BP9	BP10
m_h (GeV)	17.67	25.9	28.56	33.20	37.56	40.68	47.27	54.03	43.44	49.39
NoE($\mathcal{L}, \sigma$)	912.86	727.65	687.432	573.3	771.74	769.18	1086.62	1528.8	900.000	771.750
$e^\pm \mu^\mp$	156.934	151.874	141.094	114.84	146.44	136.2	160.54	204.94	151.226	111.163
m_Z-veto	156.934	151.874	141.094	114.84	146.44	136.2	160.54	204.94	151.226	111.163
2 b-jets	23.9	32.38	30.8	23.24	29.36	25.76	28.56	40.036	28.125	18.714
65 GeV $< m_T^H <$ 125 GeV	7.76	13.72	13.372	11.32	13.82	12.38	14.58	22.56	13.890	9.470
$\Delta m_h <$ 0.5	5.232	11.36	10.77	8.94	10.76	9.84	11.92	17.56	10.973	7.373
$m_T^{ll} <$ 62.5 GeV	5.232	11.36	10.76	8.92	10.76	9.82	11.9	17.5	10.961	7.363
$m_{bb} <$ 62.5 GeV	5.232	11.34	10.75	8.92	10.76	9.78	11.9	17.38	10.948	7.363

Table 5: Event rates of the signal with $\sqrt{s}$ = 13 TeV and integrated luminosity 300 fb^{-1} for different BPs are shown as a function of our cutflow. The pre-selection cuts are as given in Eq. (10).

In Tab. 6, we show the cutflow results by adopting the pre-selection cuts:

$$p_T(b_1) > 20 \text{ GeV}, \ p_T(b_2) > 20 \text{ GeV}, \ p_T(e/\mu) = 10/8 \text{ GeV}. \tag{11}$$

(Again, the same comments on the event kinematics of the signal apply as for the previous table.)

BP	BP1	BP2	BP3	BP4	BP5	BP6	BP7	BP8	BP9	BP10
m_h (GeV)	17.67	25.9	28.56	33.20	37.56	40.68	47.27	54.03	43.44	49.39
NoE($\mathcal{L}, \sigma$)	912.86	727.65	687.432	573.3	771.74	769.18	1086.62	1528.8	900.000	771.750
$e^\pm \mu^\mp$	156.934	151.874	141.094	114.84	146.44	136.2	160.54	204.94	151.226	111.163
m_Z-veto	156.934	151.874	141.094	114.84	146.44	136.2	160.54	204.94	151.226	111.163
2 b-jets	13.6	20.38	19.02	15.3	17.86	16.02	18.34	23.7	17.39	11.06
65 GeV $< m_T^H <$ 125 GeV	2.68	7.16	6.84	5.72	6.84	6.16	6.14	11.38	6.80	4.19
$\Delta m_h < 0.5$	1.86	5.5	5.56	4.5	5.32	4.8	5.54	8.2	5.25	3.13
$m_T^{ll} <$ 62.5 GeV	1.86	5.5	5.56	4.48	5.32	4.8	5.52	8.2	5.25	3.13
$m_{bb} <$ 62.5 GeV	1.86	5.5	5.56	4.48	5.32	4.78	5.52	8.12	5.23	3.13

Table 6: Event rates of the signal with $\sqrt{s}$ = 13 TeV and integrated luminosity 300 fb^{-1} for different BPs are shown as a function of our cutflow. The pre-selection cuts are as given in Eq. (11).

When comparing the results given in Tabs. 4, 5 and 6, particularly the number of events after requiring two tagged b-jets, it is found that the larger the p_T thresholds of the b-jets, the smaller the number of signal events which can pass the pre-selection cuts. This loss is an expected outcome for a light Higgs within the sub-50 GeV range, and it aligns with our expectations. However, it is too early to conclude that with loose cuts one can maximise the sensitivity since the effects of background have to be taken into account, which is what we are going to do next.

In Tab. 7 we show the cutflow results for the two major background processes. Here, it is noted that two mass observables, i.e., m_T^H and Δm_h, can greatly suppress background events. Another interesting observation is that, although the number of signal events is comparatively smaller with the pre-selection cut 20/20 GeV on the two tagged b-jets, the background events can be almost completely removed in this case, which eventually leads to a better sensitivity to our signal process.

Process	$Zb\bar{b}$			$t\bar{t}$		
NoE($\mathcal{L}, \sigma$)	2562000			117600		
$p_T(b_1/b_2)$ (GeV)	15/10	20/15	20/20	15/10	20/15	20/20
$e^\pm \mu^\mp$	15836.8	15836.8	15836.8	61413.5	61413.5	61413.5
m_Z-veto	15801.4	15801.4	15801.4	54511.6	54511.6	54511.6
2 b-jets	1512.57	1059.63	503.558	16871.4	13778.6	8843.26
65 GeV $< m_T^H <$ 125 GeV	272.439	154.314	33.2724	35.2954	18.8916	3.087
$\Delta m_h < 0.5$ GeV	117.072	30.0678	-	17.5266	7.6678	-
$m_T^{ll} <$ 62.5 GeV	117.072	30.0678	-	14.2366	6.125	-
$m_{bb} <$ 62.5 GeV	117.072	30.0678	-	14.2366	6.125	-

Table 7: Event rates of the two dominant background processes with $\sqrt{s}$ = 13 TeV and integrated luminosity 300 fb^{-1} as a function of our cutflow. The pre-selection cuts are as given in Eqs. (9), (10) and (11).

This is explicitly shown in Tab. 8, where the significances $\Sigma = \frac{\mathcal{N}_S}{\sqrt{\mathcal{N}_S + \mathcal{N}_B}}$[8] for 300 fb^{-1} and 3000 fb^{-1} of each BP are shown. As mentioned above, the pre-selection cut 20/20 GeV can yield

---

[8]$\mathcal{N}_S$ and $\mathcal{N}_B$ are, respectively, the number of the signal and background events after applying the kinematic cuts discussed in the text.

BP	Significance (Σ), $\mathcal{L}$ = 300 fb^{-1}			Significance (Σ), $\mathcal{L}$ = 3000 fb^{-1}		
	15/10 (GeV)	20/15 (GeV)	20/20 (GeV)	15/10 (GeV)	20/15 (GeV)	20/20 (GeV)
BP1	0.68	0.81	1.36	2.15	2.56	4.30
BP2	1.30	1.64	2.34	4.11	5.18	7.39
BP3	1.24	1.57	2.35	3.92	4.96	7.43
BP4	1.07	1.32	2.11	3.38	4.17	6.67
BP5	1.33	1.57	2.3	4.20	4.96	7.27
BP6	1.22	1.44	2.18	3.85	4.55	6.89
BP7	1.48	1.71	2.34	4.68	5.40	7.39
BP8	2.14	2.37	2.84	6.76	7.49	8.9
BP9	1.36	1.59	2.28	4.3	5.02	7.2
BP10	1.0	1.11	1.76	3.16	3.51	5.56

Table 8: Significances for our signal against the two dominant backgrounds with $\sqrt{s}$ = 13 TeV and integrated luminosity 300 fb^{-1} (left) as well as 3000 fb^{-1} (right). The pre-selection cuts are as given in Eqs. (9), (10) and (11).

a better significance, so it is the one we would recommend for the actual analysis. Altogether, although (some of) these BPs might be difficult to discover or rule out at Run 3 of the LHC, all of these BPs are within full reach of the HL-LHC.

5   Conclusions

The Type-I is an intriguing realisation of the 2HDM as it allows for the so-called inverted mass hierarchy scenario, wherein the Higgs boson discovered at the LHC on 4 July 2012 can be identified as the heaviest CP-even Higgs state of this construct, H, with a mass of 125 GeV or so and couplings to fermions and gauge bosons similar to those predicted in the SM. Such a configuration specifically implies that there is then a lighter CP-even Higgs state, h, into pairs of which the heavy one can decay: i.e., via $H \to hh$. Needless to say, this can be realised without contradicting any of the theoretical requirements of self-consistency of the 2HDM or current experimental results, whether coming for measurements of the discovered Higgs boson or null searches for companions to it. In fact, the latter have primarily been concentrating on other realisations of the 2HDM, where only the standard mass hierarchy is actually possible (i.e., $m_h \approx 125$ GeV $< m_H$), thereby altogether missing out on the possibility of optimising searches for very light neutral Higgs states in general. Specifically, here, by looking for $H \to hh$ signals in the 2HDM Type-I, we have concentrated on the following mass range: 15 GeV $< m_h < m_H/2$.

The production of the heavy CP-even Higgs state (the SM-like Higgs boson) at the LHC was pursued via gluon-gluon fusion, $gg \to H$, indeed, the dominant channel, while we have focused on the $hh \to b\bar{b}\tau\tau$ decay pattern, where the two heavy leptons where tagged through their (different flavour) electron and muon decays. By performing a sophisticated MC analysis of signal versus background, we have shown that both Run 3 of the CERN machine and its HL-LHC phase can offer sensitivity to this 2HDM Type-I signal, in the presence of very low mass trigger thresholds (on the electrons and muons) already implemented for Run 3 and also possible at the HL-LHC. We have done so by adopting several BPs capturing representative m_h values over the aforementioned interval after a fine scanning of the whole 2HDM Type-I parameter space, of which they are therefore representative examples amenable to further scrutiny by the LHC collaborations. Finally notice that, if the collision energy of the LHC increases from 13 TeV to 14 TeV, the production rate of the signal process $gg \to H$ can increase by 10%, as

shown in [65] (with the dominant backgrounds, $t\bar{t}$ and $Zb\bar{b}$, scaling similarly or less), lending further scope to our analysis in the near future.

Appendix

Additional kinematic variables can serve to further discriminate the Higgs signal from background events in the low mass range. Leptons arising from light Higgs decays demonstrate small opening angles, whereas those from $t\bar{t}$ (large missing transverse momentum) and $Z(\to \tau\tau)b\bar{b}$ (emitted back-to-back) would be large. Therefore, requiring a small opening angle between the two leptons, along with a small angle between the missing transverse momentum and the leptons would reduce the background processes. This is exemplified in Fig. 14. However, we did not pursue this here.
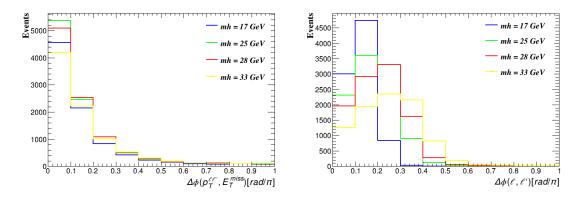

Figure 14: Opening angles distributions between the two leptons $\Delta\phi(l, l')$ (left panel) and between the missing transverse momentum and the leptons $\Delta\phi(p_T^{ll'}, E_T^{miss})$ (right panel) for the signal, with $(ll' = e^\pm \mu^\mp)$.

Acknowledgements

References

[1] Georges Aad et al. Observation of a new particle in the search for the Standard Model Higgs boson with the ATLAS detector at the LHC. *Phys. Lett. B*, 716:1–29, 2012.

[2] Serguei Chatrchyan et al. Observation of a New Boson at a Mass of 125 GeV with the CMS Experiment at the LHC. *Phys. Lett. B*, 716:30–61, 2012.

[3] F. Englert and R. Brout. Broken Symmetry and the Mass of Gauge Vector Mesons. *Phys. Rev. Lett.*, 13:321–323, 1964.

[4] Peter W. Higgs. Broken Symmetries and the Masses of Gauge Bosons. *Phys. Rev. Lett.*, 13:508–509, 1964.

[5] A detailed map of Higgs boson interactions by the ATLAS experiment ten years after the discovery. *Nature*, 607(7917):52–59, 2022. [Erratum: Nature 612, E24 (2022)].

[6] Armen Tumasyan et al. A portrait of the Higgs boson by the CMS experiment ten years after the discovery. *Nature*, 607(7917):60–68, 2022.

[7] A. Liss and J. Nielsen. Physics at a High-Luminosity LHC with ATLAS. 7 2013.

[8] Projected Performance of an Upgraded CMS Detector at the LHC and HL-LHC: Contribution to the Snowmass Process. In *Snowmass 2013: Snowmass on the Mississippi*, 7 2013.

[9] Stefano Moretti and Shaaban Khalil. *Supersymmetry Beyond Minimality: From Theory to Experiment*. CRC Press, 2019.

[10] A. Dedes, C. Hugonie, S. Moretti, and K. Tamvakis. Phenomenology of a new minimal supersymmetric extension of the standard model. *Phys. Rev. D*, 63:055009, 2001.

[11] Bogdan A. Dobrescu and Konstantin T. Matchev. Light axion within the next-to-minimal supersymmetric standard model. *JHEP*, 09:031, 2000.

[12] Ulrich Ellwanger, John F. Gunion, Cyril Hugonie, and Stefano Moretti. Towards a no lose theorem for NMSSM Higgs discovery at the LHC. 5 2003.

[13] Radovan Dermisek and John F. Gunion. Escaping the large fine tuning and little hierarchy problems in the next to minimal supersymmetric model and $h \to aa$ decays. *Phys. Rev. Lett.*, 95:041801, 2005.

[14] Maxim Pospelov, Adam Ritz, and Mikhail B. Voloshin. Secluded WIMP Dark Matter. *Phys. Lett. B*, 662:53–61, 2008.

[15] Patrick Draper, Tao Liu, Carlos E. M. Wagner, Lian-Tao Wang, and Hao Zhang. Dark Light Higgs. *Phys. Rev. Lett.*, 106:121805, 2011.

[16] Seyda Ipek, David McKeen, and Ann E. Nelson. A Renormalizable Model for the Galactic Center Gamma Ray Excess from Dark Matter Annihilation. *Phys. Rev. D*, 90(5):055021, 2014.

[17] Abdesslam Arhrib, Yue-Lin Sming Tsai, Qiang Yuan, and Tzu-Chiang Yuan. An Updated Analysis of Inert Higgs Doublet Model in light of the Recent Results from LUX, PLANCK, AMS-02 and LHC. *JCAP*, 06:030, 2014.

[18] Stefano Profumo, Michael J. Ramsey-Musolf, and Gabe Shaughnessy. Singlet Higgs phenomenology and the electroweak phase transition. *JHEP*, 08:010, 2007.

[19] Nikita Blinov, Jonathan Kozaczuk, David E. Morrissey, and Carlos Tamarit. Electroweak Baryogenesis from Exotic Electroweak Symmetry Breaking. *Phys. Rev. D*, 92(3):035012, 2015.

[20] T. D. Lee. A Theory of Spontaneous T Violation. *Phys. Rev. D*, 8:1226–1239, 1973.

[21] G. C. Branco, P. M. Ferreira, L. Lavoura, M. N. Rebelo, Marc Sher, and Joao P. Silva. Theory and phenomenology of two-Higgs-doublet models. *Phys. Rept.*, 516:1–102, 2012.

[22] Abdesslam Arhrib, Rachid Benbrik, Stefano Moretti, Abdessamad Rouchad, Qi-Shu Yan, and Xianhui Zhang. Multi-photon production in the Type-I 2HDM. *JHEP*, 07:007, 2018.

[23] Alejandro Celis, Victor Ilisie, and Antonio Pich. LHC constraints on two-Higgs doublet models. *JHEP*, 07:053, 2013.

[24] Benjamin Grinstein and Patipan Uttayarat. Carving Out Parameter Space in Type-II Two Higgs Doublets Model. *JHEP*, 06:094, 2013. [Erratum: JHEP 09, 110 (2013)].

[25] Chien-Yi Chen, S. Dawson, and Marc Sher. Heavy Higgs Searches and Constraints on Two Higgs Doublet Models. *Phys. Rev. D*, 88:015018, 2013. [Erratum: Phys.Rev.D 88, 039901 (2013)].

[26] V. Khachatryan et al. Search for light bosons in decays of the 125 GeV Higgs boson in proton-proton collisions at $\sqrt{s}$ = 8 TeV. *JHEP*, 10:076, 2017.

[27] Albert M Sirunyan et al. Search for light pseudoscalar boson pairs produced from decays of the 125 GeV Higgs boson in final states with two muons and two nearby tracks in pp collisions at $\sqrt{s}$ = 13 TeV. *Phys. Lett. B*, 800:135087, 2020.

[28] Georges Aad et al. Search for Higgs bosons decaying to aa in the $\mu\mu\tau\tau$ final state in pp collisions at $\sqrt{s}$ = 8 TeV with the ATLAS experiment. *Phys. Rev. D*, 92(5):052002, 2015.

[29] Albert M Sirunyan et al. Search for an exotic decay of the Higgs boson to a pair of light pseudoscalars in the final state of two muons and two τ leptons in proton-proton collisions at $\sqrt{s}$ = 13 TeV. *JHEP*, 11:018, 2018.

[30] Albert M Sirunyan et al. Search for a light pseudoscalar Higgs boson in the boosted $\mu\mu\tau\tau$ final state in proton-proton collisions at $\sqrt{s}$ = 13 TeV. *JHEP*, 08:139, 2020.

[31] Search for exotic decays of the Higgs boson to a pair of new light bosons in the $\mu\mu bb$ final state at $\sqrt{s}$ = 13 TeV with the full Run 2 dataset. 2022.

[32] Search for exotic Higgs boson decays to a pair of pseudoscalars in the $\mu\mu$bb and $\tau\tau$bb final states in proton-proton collisions with the CMS experiment. 2023.

[33] Albert M Sirunyan et al. Search for Higgs boson pair production in events with two bottom quarks and two tau leptons in proton–proton collisions at $\sqrt{s}$ =13TeV. *Phys. Lett. B*, 778:101–127, 2018.

[34] Albert M Sirunyan et al. Search for an exotic decay of the Higgs boson to a pair of light pseudoscalars in the final state with two b quarks and two τ leptons in proton-proton collisions at $\sqrt{s}$ = 13 TeV. *Phys. Lett. B*, 785:462, 2018.

[35] Morad Aaboud et al. Search for Higgs boson decays to beyond-the-Standard-Model light bosons in four-lepton events with the ATLAS detector at $\sqrt{s}$ = 13 TeV. *JHEP*, 06:166, 2018.

[36] Serguei Chatrchyan et al. Search for a Non-Standard-Model Higgs Boson Decaying to a Pair of New Light Bosons in Four-Muon Final States. *Phys. Lett. B*, 726:564–586, 2013.

[37] V. Khachatryan et al. A search for pair production of new light bosons decaying into muons. *Phys. Lett. B*, 752:146–168, 2016.

[38] Albert M Sirunyan et al. A search for pair production of new light bosons decaying into muons in proton-proton collisions at 13 TeV. *Phys. Lett. B*, 796:131–154, 2019.

[39] Georges Aad et al. Search for Higgs bosons decaying into new spin-0 or spin-1 particles in four-lepton final states with the ATLAS detector with 139 fb^{-1} of pp collision data at $\sqrt{s}$ = 13 TeV. *JHEP*, 03:041, 2022.

[40] F. Gianotti et al. Physics potential and experimental challenges of the LHC luminosity upgrade. *Eur. Phys. J. C*, 39:293–333, 2005.

[41] Abdesslam Arhrib, Rachid Benbrik, and Cheng-Wei Chiang. Probing triple Higgs couplings of the Two Higgs Doublet Model at Linear Collider. *Phys. Rev. D*, 77:115013, 2008.

[42] Shinya Kanemura, Mariko Kikuchi, and Kei Yagyu. Fingerprinting the extended Higgs sector using one-loop corrected Higgs boson couplings and future precision measurements. *Nucl. Phys. B*, 896:80–137, 2015.

[43] Sheldon L. Glashow and Steven Weinberg. Natural Conservation Laws for Neutral Currents. *Phys. Rev. D*, 15:1958, 1977.

[44] Shinya Kanemura, Takahiro Kubota, and Eiichi Takasugi. Lee-Quigg-Thacker bounds for Higgs boson masses in a two doublet model. *Phys. Lett. B*, 313:155–160, 1993.

[45] Andrew G. Akeroyd, Abdesslam Arhrib, and El-Mokhtar Naimi. Note on tree level unitarity in the general two Higgs doublet model. *Phys. Lett. B*, 490:119–124, 2000.

[46] Abdesslam Arhrib. Unitarity constraints on scalar parameters of the standard and two Higgs doublets model. In *Workshop on Noncommutative Geometry, Superstrings and Particle Physics*, 12 2000.

[47] Nilendra G. Deshpande and Ernest Ma. Pattern of Symmetry Breaking with Two Higgs Doublets. *Phys. Rev. D*, 18:2574, 1978.

[48] David Eriksson, Johan Rathsman, and Oscar Stal. 2HDMC: Two-Higgs-Doublet Model Calculator Physics and Manual. *Comput. Phys. Commun.*, 181:189–205, 2010.

[49] Philip Bechtle, Daniel Dercks, Sven Heinemeyer, Tobias Klingl, Tim Stefaniak, Georg Weiglein, and Jonas Wittbrodt. HiggsBounds-5: Testing Higgs Sectors in the LHC 13 TeV Era. *Eur. Phys. J. C*, 80(12):1211, 2020.

[50] Philip Bechtle, Sven Heinemeyer, Tobias Klingl, Tim Stefaniak, Georg Weiglein, and Jonas Wittbrodt. HiggsSignals-2: Probing new physics with precision Higgs measurements in the LHC 13 TeV era. *Eur. Phys. J. C*, 81(2):145, 2021.

[51] Hong-Jian He, Nir Polonsky, and Shu-fang Su. Extra families, Higgs spectrum and oblique corrections. *Phys. Rev. D*, 64:053004, 2001.

[52] W. Grimus, L. Lavoura, O. M. Ogreid, and P. Osland. The Oblique parameters in multi-Higgs-doublet models. *Nucl. Phys. B*, 801:81–96, 2008.

[53] Howard E. Haber and Deva O'Neil. Basis-independent methods for the two-Higgs-doublet model III: The CP-conserving limit, custodial symmetry, and the oblique parameters S, T, U. *Phys. Rev. D*, 83:055017, 2011.

[54] P. A. Zyla et al. Review of Particle Physics. *PTEP*, 2020(8):083C01, 2020.

[55] F. Mahmoudi. SuperIso v2.3: A Program for calculating flavor physics observables in Supersymmetry. *Comput. Phys. Commun.*, 180:1579–1613, 2009.

[56] Y. Amhis et al. Averages of b-hadron, c-hadron, and τ-lepton properties as of summer 2016. *Eur. Phys. J. C*, 77(12):895, 2017.

[57] Roel Aaij et al. Measurement of the $B_s^0 \to \mu^+\mu^-$ decay properties and search for the $B^0 \to \mu^+\mu^-$ and $B_s^0 \to \mu^+\mu^-\gamma$ decays. *Phys. Rev. D*, 105(1):012010, 2022.

[58] R. Aaij et al. Analysis of Neutral B-Meson Decays into Two Muons. *Phys. Rev. Lett.*, 128(4):041801, 2022.

[59] Armen Tumasyan et al. Measurement of the $B_S^0 \to \mu^+\mu^-$ decay properties and search for the $B^0 \to \mu^+\mu^-$ decay in proton-proton collisions at $\sqrt{s} = 13$ TeV. *Phys. Lett. B*, 842:137955, 2023.

[60] Georges Aad et al. Evidence of off-shell Higgs boson production from ZZ leptonic decay channels and constraints on its total width with the ATLAS detector. 4 2023.

[61] Armen Tumasyan et al. Measurement of the Higgs boson width and evidence of its off-shell contributions to ZZ production. *Nature Phys.*, 18(11):1329–1334, 2022.

[62] Robert V. Harlander, Stefan Liebler, and Hendrik Mantler. SusHi: A program for the calculation of Higgs production in gluon fusion and bottom-quark annihilation in the Standard Model and the MSSM. *Comput. Phys. Commun.*, 184:1605–1617, 2013.

[63] Robert V. Harlander, Stefan Liebler, and Hendrik Mantler. SusHi Bento: Beyond NNLO and the heavy-top limit. *Comput. Phys. Commun.*, 212:239–257, 2017.

[64] Robert V. Harlander and William B. Kilgore. Next-to-next-to-leading order Higgs production at hadron colliders. *Phys. Rev. Lett.*, 88:201801, 2002.

[65] Charalampos Anastasiou, Claude Duhr, Falko Dulat, Franz Herzog, and Bernhard Mistlberger. Higgs Boson Gluon-Fusion Production in QCD at Three Loops. *Phys. Rev. Lett.*, 114:212001, 2015.

[66] M. Cepeda et al. Report from Working Group 2: Higgs Physics at the HL-LHC and HE-LHC. *CERN Yellow Rep. Monogr.*, 7:221–584, 2019.

[67] Combination of searches for invisible decays of the Higgs boson using 139 fb−1 of proton-proton collision data at s=13 TeV collected with the ATLAS experiment. *Phys. Lett. B*, 842:137963, 2023.

[68] A search for decays of the Higgs boson to invisible particles in events with a top-antitop quark pair or a vector boson in proton-proton collisions at $\sqrt{s} = 13$ TeV. 3 2023.

[69] S. Schael et al. Search for neutral MSSM Higgs bosons at LEP. *Eur. Phys. J. C*, 47:547–587, 2006.

[70] Georges Aad et al. Search for new phenomena in events with at least three photons collected in pp collisions at $\sqrt{s} = 8$ TeV with the ATLAS detector. *Eur. Phys. J. C*, 76(4):210, 2016.

[71] Kaoru Hagiwara, Tong Li, Kentarou Mawatari, and Junya Nakamura. TauDecay: a library to simulate polarized tau decays via FeynRules and MadGraph5. *Eur. Phys. J. C*, 73:2489, 2013.

[72] J. Alwall, R. Frederix, S. Frixione, V. Hirschi, F. Maltoni, O. Mattelaer, H. S. Shao, T. Stelzer, P. Torrielli, and M. Zaro. The automated computation of tree-level and next-to-leading order differential cross sections, and their matching to parton shower simulations. *JHEP*, 07:079, 2014.

[73] Fernando Febres Cordero, L. Reina, and D. Wackeroth. W- and Z-boson production with a massive bottom-quark pair at the Large Hadron Collider. *Phys. Rev. D*, 80:034015, 2009.

[74] T. Binoth et al. The SM and NLO Multileg Working Group: Summary report. In *6th Les Houches Workshop on Physics at TeV Colliders*, pages 21–189, 3 2010.

[75] Torbjorn Sjostrand, Stephen Mrenna, and Peter Z. Skands. PYTHIA 6.4 Physics and Manual. *JHEP*, 05:026, 2006.

[76] J. de Favereau, C. Delaere, P. Demin, A. Giammanco, V. Lemaître, A. Mertens, and M. Selvaggi. DELPHES 3, A modular framework for fast simulation of a generic collider experiment. *JHEP*, 02:057, 2014.

[77] Eric Conte, Benjamin Fuks, and Guillaume Serret. MadAnalysis 5, A User-Friendly Framework for Collider Phenomenology. *Comput. Phys. Commun.*, 184:222–256, 2013.

[78] Vardan Khachatryan et al. The CMS trigger system. *JINST*, 12(01):P01020, 2017.

[79] A. M. Sirunyan et al. Performance of reconstruction and identification of τ leptons decaying to hadrons and ν_τ in pp collisions at $\sqrt{s}$ = 13 TeV. *JINST*, 13(10):P10005, 2018.

[80] Swagata Mukherjee. Data Scouting and Data Parking with the CMS High level Trigger. *PoS*, EPS-HEP2019:139, 2020.

[81] Robert Bainbridge. Recording and reconstructing 10 billion unbiased b hadron decays in CMS. *EPJ Web Conf.*, 245:01025, 2020.

[82] Matteo Cacciari, Gavin P. Salam, and Gregory Soyez. The anti-k_t jet clustering algorithm. *JHEP*, 04:063, 2008.

[83] Yuri L. Dokshitzer, G. D. Leder, S. Moretti, and B. R. Webber. Better jet clustering algorithms. *JHEP*, 08:001, 1997.

[84] M. Wobisch and T. Wengler. Hadronization corrections to jet cross-sections in deep inelastic scattering. In *Workshop on Monte Carlo Generators for HERA Physics (Plenary Starting Meeting)*, pages 270–279, 4 1998.

[85] Serguei Chatrchyan et al. Identification of b-Quark Jets with the CMS Experiment. *JINST*, 8:P04013, 2013.

[86] A. M. Sirunyan et al. Identification of heavy-flavour jets with the CMS detector in pp collisions at 13 TeV. *JINST*, 13(05):P05011, 2018.

[87] Antimo Cagnotta, Francesco Carnevali, and Agostino De Iorio. Machine Learning Applications for Jet Tagging in the CMS Experiment. *Appl. Sciences*, 12(20):10574, 2022.